The Astrophysical Journal, 723:1082–1096, 2010 November 10 doi:10.1088/0004-637X/723/2/1082

FERMI LARGE AREA TELESCOPE CONSTRAINTS ON THE GAMMA-RAY OPACITY OF THE UNIVERSE

A. A. Abdo[1,2], M. Ackermann[3], M. Ajello[3], A. Allafort[3], W. B. Atwood[4], L. Baldini[5], J. Ballet[6], G. Barbiellini[7,8], M. G. Baring[9], D. Bastieri[10,11], B. M. Baughman[12], K. Bechtol[3], R. Bellazzini[5], B. Berenji[3], P. N. Bhat[13], R. D. Blandford[3], E. D. Bloom[3], E. Bonamente[14,15], A. W. Borgland[3], A. Bouvier[3,61], T. J. Brandt[12,16], J. Bregeon[5], A. Brez[5], M. S. Briggs[13], M. Brigida[17,18], P. Bruel[19], R. Buehler[3], T. H. Burnett[20], S. Buson[10,11], G. A. Caliandro[21], R. A. Cameron[3], P. A. Caraveo[22], S. Carrigan[11], J. M. Casandjian[6], E. Cavazzuti[23], C. Cecchi[14,15], Ö. Çelik[24,25,26], E. Charles[3], A. Chekhtman[1,27], A. W. Chen[22,61], C. C. Cheung[1,2], J. Chiang[3], S. Ciprini[15], R. Claus[3], J. Cohen-Tanugi[28], V. Connaughton[13], J. Conrad[29,30,59], L. Costamante[3], C. D. Dermer[1], A. de Angelis[31], F. de Palma[17,18], S. W. Digel[3], B. L. Dingus[32], E. do Couto e Silva[3], P. S. Drell[3], R. Dubois[3], C. Favuzzi[17,18], S. J. Fegan[19], J. Finke[1,2], P. Fortin[19], Y. Fukazawa[33], S. Funk[3], P. Fusco[17,18], F. Gargano[18], D. Gasparrini[23], N. Gehrels[24], S. Germani[14,15], N. Giglietto[17,18], R. C. Gilmore[4], P. Giommi[23], F. Giordano[17,18], M. Giroletti[34], T. Glanzman[3], G. Godfrey[3], J. Granot[35], J. Greiner[36], I. A. Grenier[6], J. E. Grove[1], S. Guiriec[13], M. Gustafsson[10], D. Hadasch[37], M. Hayashida[3], E. Hays[24], D. Horan[19], R. E. Hughes[12], G. Jóhannesson[3], A. S. Johnson[3], R. P. Johnson[4], W. N. Johnson[1], T. Kamae[3], H. Katagiri[33], J. Kataoka[38], J. Knödlseder[16], D. Kocevski[3], M. Kuss[5], J. Lande[3], L. Latronico[5], S.-H. Lee[3], M. Llena Garde[29,30], F. Longo[7,8], F. Loparco[17,18], B. Lott[39,40], M. N. Lovellette[1], P. Lubrano[14,15], A. Makeev[1,27], M. N. Mazziotta[18], W. McConville[24,41], J. E. McEnery[24,41], S. McGlynn[30,42], J. Mehault[28], P. Mészáros[43], P. F. Michelson[3], T. Mizuno[33], A. A. Moiseev[25,41], C. Monte[17,18], M. E. Monzani[3], E. Moretti[7,8], A. Morselli[44], I. V. Moskalenko[3], S. Murgia[3], T. Nakamori[38], M. Naumann-Godo[6], P. L. Nolan[3], J. P. Norris[45], E. Nuss[28], M. Ohno[46], T. Ohsugi[47], A. Okumura[46], N. Omodei[3], E. Orlando[36], J. F. Ormes[45], M. Ozaki[46], D. Paneque[3], J. H. Panetta[3], D. Parent[1,27], V. Pelassa[28], M. Pepe[14,15], M. Pesce-Rollins[5], F. Piron[28], T. A. Porter[3], J. R. Primack[4], S. Rainò[17,18,61], R. Rando[10,11], M. Razzano[5], S. Razzaque[1,2,61], A. Reimer[3,48,61], O. Reimer[3,48], L. C. Reyes[49,61], J. Ripken[29,30], S. Ritz[4], R. W. Romani[3], M. Roth[20], H. F.-W. Sadrozinski[4], D. Sanchez[19], A. Sander[12], J. D. Scargle[50], T. L. Schalk[4], C. Sgrò[5], M. S. Shaw[3], E. J. Siskind[51], P. D. Smith[12], G. Spandre[5], P. Spinelli[17,18], F. W. Stecker[24], M. S. Strickman[1], D. J. Suson[52], H. Tajima[3], H. Takahashi[47], T. Takahashi[46], T. Tanaka[3], J. B. Thayer[3], J. G. Thayer[3], D. J. Thompson[24], L. Tibaldo[6,10,11,60], D. F. Torres[21,37], G. Tosti[14,15], A. Tramacere[3,53,54], Y. Uchiyama[3], T. L. Usher[3], J. Vandenbroucke[3], V. Vasileiou[25,26], N. Vilchez[16], V. Vitale[44,55], A. von Kienlin[36], A. P. Waite[3], P. Wang[3], C. Wilson-Hodge[56], B. L. Winer[12], K. S. Wood[1], R. Yamazaki[57], Z. Yang[29,30], T. Ylinen[30,42,58], and M. Ziegler[4]

[1] Space Science Division, Naval Research Laboratory, Washington, DC 20375, USA
[2] National Research Council Research Associate, National Academy of Sciences, Washington, DC 20001, USA
[3] W. W. Hansen Experimental Physics Laboratory, Kavli Institute for Particle Astrophysics and Cosmology, Department of Physics and SLAC National Accelerator Laboratory, Stanford University, Stanford, CA 94305, USA
[4] Santa Cruz Institute for Particle Physics, Department of Physics and Department of Astronomy and Astrophysics, University of California at Santa Cruz, Santa Cruz, CA 95064, USA
[5] Istituto Nazionale di Fisica Nucleare, Sezione di Pisa, I-56127 Pisa, Italy
[6] Laboratoire AIM, CEA-IRFU/CNRS/Université Paris Diderot, Service d'Astrophysique, CEA Saclay, 91191 Gif sur Yvette, France
[7] Istituto Nazionale di Fisica Nucleare, Sezione di Trieste, I-34127 Trieste, Italy
[8] Dipartimento di Fisica, Università di Trieste, I-34127 Trieste, Italy
[9] Rice University, Department of Physics and Astronomy, MS-108, P. O. Box 1892, Houston, TX 77251, USA
[10] Istituto Nazionale di Fisica Nucleare, Sezione di Padova, I-35131 Padova, Italy
[11] Dipartimento di Fisica "G. Galilei," Università di Padova, I-35131 Padova, Italy
[12] Department of Physics, Center for Cosmology and Astro-Particle Physics, The Ohio State University, Columbus, OH 43210, USA
[13] Center for Space Plasma and Aeronomic Research (CSPAR), University of Alabama in Huntsville, Huntsville, AL 35899, USA
[14] Istituto Nazionale di Fisica Nucleare, Sezione di Perugia, I-06123 Perugia, Italy
[15] Dipartimento di Fisica, Università degli Studi di Perugia, I-06123 Perugia, Italy
[16] Centre d'Étude Spatiale des Rayonnements, CNRS/UPS, BP 44346, F-30128 Toulouse Cedex 4, France
[17] Dipartimento di Fisica "M. Merlin" dell'Università e del Politecnico di Bari, I-70126 Bari, Italy
[18] Istituto Nazionale di Fisica Nucleare, Sezione di Bari, 70126 Bari, Italy
[19] Laboratoire Leprince-Ringuet, École polytechnique, CNRS/IN2P3, Palaiseau, France
[20] Department of Physics, University of Washington, Seattle, WA 98195-1560, USA
[21] Institut de Ciencies de l'Espai (IEEC-CSIC), Campus UAB, 08193 Barcelona, Spain
[22] INAF-Istituto di Astrofisica Spaziale e Fisica Cosmica, I-20133 Milano, Italy
[23] Agenzia Spaziale Italiana (ASI) Science Data Center, I-00044 Frascati (Roma), Italy
[24] NASA Goddard Space Flight Center, Greenbelt, MD 20771, USA
[25] Center for Research and Exploration in Space Science and Technology (CRESST) and NASA Goddard Space Flight Center, Greenbelt, MD 20771, USA
[26] Department of Physics and Center for Space Sciences and Technology, University of Maryland Baltimore County, Baltimore, MD 21250, USA
[27] George Mason University, Fairfax, VA 22030, USA
[28] Laboratoire de Physique Théorique et Astroparticules, Université Montpellier 2, CNRS/IN2P3, Montpellier, France
[29] Department of Physics, Stockholm University, AlbaNova, SE-106 91 Stockholm, Sweden
[30] The Oskar Klein Centre for Cosmoparticle Physics, AlbaNova, SE-106 91 Stockholm, Sweden
[31] Dipartimento di Fisica, Università di Udine and Istituto Nazionale di Fisica Nucleare, Sezione di Trieste, Gruppo Collegato di Udine, I-33100 Udine, Italy
[32] Los Alamos National Laboratory, Los Alamos, NM 87545, USA
[33] Department of Physical Sciences, Hiroshima University, Higashi-Hiroshima, Hiroshima 739-8526, Japan
[34] INAF Istituto di Radioastronomia, 40129 Bologna, Italy
[35] Centre for Astrophysics Research, Science and Technology Research Institute, University of Hertfordshire, Hatfield AL10 9AB, UK
[36] Max-Planck Institut für extraterrestrische Physik, 85748 Garching, Germany

[37] Institució Catalana de Recerca i Estudis Avançats (ICREA), Barcelona, Spain
[38] Research Institute for Science and Engineering, Waseda University, 3-4-1, Okubo, Shinjuku, Tokyo, 169-8555 Japan
[39] CNRS/IN2P3, Centre d'Études Nucléaires Bordeaux Gradignan, UMR 5797, Gradignan, 33175, France
[40] Université de Bordeaux, Centre d'Études Nucléaires Bordeaux Gradignan, UMR 5797, Gradignan, 33175, France
[41] Department of Physics and Department of Astronomy, University of Maryland, College Park, MD 20742, USA
[42] Department of Physics, Royal Institute of Technology (KTH), AlbaNova, SE-106 91 Stockholm, Sweden
[43] Department of Astronomy and Astrophysics, Pennsylvania State University, University Park, PA 16802, USA
[44] Istituto Nazionale di Fisica Nucleare, Sezione di Roma "Tor Vergata," I-00133 Roma, Italy
[45] Department of Physics and Astronomy, University of Denver, Denver, CO 80208, USA
[46] Institute of Space and Astronautical Science, JAXA, 3-1-1 Yoshinodai, Sagamihara, Kanagawa 229-8510, Japan
[47] Hiroshima Astrophysical Science Center, Hiroshima University, Higashi-Hiroshima, Hiroshima 739-8526, Japan
[48] Institut für Astro- und Teilchenphysik and Institut für Theoretische Physik, Leopold-Franzens-Universität Innsbruck, A-6020 Innsbruck, Austria
[49] Kavli Institute for Cosmological Physics, University of Chicago, Chicago, IL 60637, USA
[50] Space Sciences Division, NASA Ames Research Center, Moffett Field, CA 94035-1000, USA
[51] NYCB Real-Time Computing Inc., Lattingtown, NY 11560-1025, USA
[52] Department of Chemistry and Physics, Purdue University Calumet, Hammond, IN 46323-2094, USA
[53] Consorzio Interuniversitario per la Fisica Spaziale (CIFS), I-10133 Torino, Italy
[54] INTEGRAL Science Data Centre, CH-1290 Versoix, Switzerland
[55] Dipartimento di Fisica, Università di Roma "Tor Vergata," I-00133 Roma, Italy
[56] NASA Marshall Space Flight Center, Huntsville, AL 35812, USA
[57] Department of Physics and Mathematics, Aoyama Gakuin University, Sagamihara, Kanagawa, 252-5258, Japan
[58] School of Pure and Applied Natural Sciences, University of Kalmar, SE-391 82 Kalmar, Sweden
Received 2010 May 6; accepted 2010 August 24; published 2010 October 19

ABSTRACT

The extragalactic background light (EBL) includes photons with wavelengths from ultraviolet to infrared, which are effective at attenuating gamma rays with energy above ∼10 GeV during propagation from sources at cosmological distances. This results in a redshift- and energy-dependent attenuation of the γ-ray flux of extragalactic sources such as blazars and gamma-ray bursts (GRBs). The Large Area Telescope on board *Fermi* detects a sample of γ-ray blazars with redshift up to $z \sim 3$, and GRBs with redshift up to $z \sim 4.3$. Using photons above 10 GeV collected by *Fermi* over more than one year of observations for these sources, we investigate the effect of γ-ray flux attenuation by the EBL. We place upper limits on the γ-ray opacity of the universe at various energies and redshifts and compare this with predictions from well-known EBL models. We find that an EBL intensity in the optical–ultraviolet wavelengths as great as predicted by the "baseline" model of Stecker et al. can be ruled out with high confidence.

Key words: diffuse radiation – dust, extinction – gamma rays: general

Online-only material: color figures

1. INTRODUCTION

The *Fermi* Gamma Ray Space Telescope was launched on 2008 June 11, to provide an unprecedented view of the γ-ray universe. The main instrument on board *Fermi*, the Large Area Telescope (LAT), offers a broader bandpass (∼20 MeV to over 300 GeV; Atwood et al. 2009) and improved sensitivity (by greater than an order of magnitude) than that of its predecessor instrument EGRET on board the *Compton Gamma Ray Observatory* (Thompson et al. 1993), and the Italian Space Agency satellite *AGILE* (Tavani et al. 2008), which was launched in 2007. LAT observes the full sky every 3 hr in survey mode leading to a broadly uniform exposure with less than ∼15% variation. The Gamma-ray Burst Monitor, the lower energy (∼8 keV–40 MeV) instrument on board *Fermi*, observes the full un-occulted sky at all times and provides alerts for transient sources such as gamma-ray bursts (GRBs).

A major science goal of *Fermi* is to probe the opacity of the universe to high-energy (HE) γ-rays as they propagate from their sources to Earth. Such energetic photons are subject to absorption by production of electron–positron (e^-e^+) pairs while interacting with low-energy cosmic background photons (Nishikov 1961; Gould & Shréder 1966; Fazio & Stecker 1970) if above the interaction threshold: $\epsilon_{\rm thr} = (2m_ec^2)^2/(2E(1-\mu))$ where ϵ and E denote the energies of the background photon and γ-ray, respectively, in the comoving frame of the interaction, m_ec^2 is the rest mass electron energy, and $\theta = \arccos(\mu)$ is the interaction angle. Because of the sharply peaked cross section close to threshold, most interactions are centered around $\epsilon^* \approx 0.8(E/\mathrm{TeV})^{-1}$ eV for a smooth broadband spectrum. Thus, the extragalactic background light (EBL) at UV through optical wavelengths constitutes the main source of opacity for γ-rays from extragalactic sources (active galactic nuclei (AGNs) and GRBs) in the LAT energy range. The effect of absorption of HE γ-rays is then reflected in an energy- and redshift-dependent softening of the observed spectrum from a distant γ-ray source. The observation, or absence, of such spectral features at HEs, for a source at redshift z can be used to constrain the $\gamma\gamma \rightarrow e^+e^-$ pair production optical depth, $\tau_{\gamma\gamma}(E, z)$.

The EBL is dominated by radiation from stars, directly from their surface and via reprocessing by dust in their host galaxies, that accumulated over cosmological evolution. Knowledge of its intensity variation with time would probe models of galaxy and star formation. The intensity of the EBL from the near-IR to ultraviolet is thought to be dominated by direct starlight emission out to large redshifts and to a lesser extent by

[59] Royal Swedish Academy of Sciences Research Fellow, funded by a grant from the K. A. Wallenberg Foundation.
[60] Partially supported by the International Doctorate on Astroparticle Physics (IDAPP) program.
[61] Corresponding authors: md.razzaque.ctr.bg@nrl.navy.mil, bouvier@stanford.edu, anita.reimer@uibk.ac.at, silvia.raino@ba.infn.it, chen@iasf-milano.inaf.it, lreyes@kicp.uchicago.edu.

optically bright AGNs. At longer wavelengths, the infrared background is produced by thermal radiation from dust which is heated by starlight, and also emission from polycyclic aromatic hydrocarbons (see, e.g., Driver et al. 2008).

Direct measurements of the EBL are difficult due to contamination by foreground zodiacal and Galactic light (e.g., Hauser & Dwek 2001), and galaxy counts result in a lower limit since the number of unresolved sources is unknown (e.g., Madau & Pozzetti 2000). Furthermore, evolution of the EBL density in the past epochs ($z > 0$) that is required to calculate the γ-ray flux attenuation from distant sources cannot be addressed by measuring the EBL density at the present epoch ($z = 0$). Hence, several approaches have been developed to calculate the EBL density as a function of redshift. The models encompass different degrees of complexity, observational constraints, and data inputs. Unfortunately, the available direct EBL measurements do not constrain these models strongly at optical-UV wavelengths due to the large scatter in the data points. A description of the different models is beyond the scope of this work; we refer the reader to the original works on the various EBL models (e.g., Salamon & Stecker 1998; Stecker et al. 2006; Kneiske et al. 2002, 2004; Primack et al. 2005; Gilmore et al. 2009; Franceschini et al. 2008; Razzaque et al. 2009; Finke et al. 2010). We note that all recent EBL models, and in particular all models used in this paper, use almost identical parameters of a ΛCDM cosmology model.

For the analyses presented in this work, we have made use of the optical depth values $\tau(E, z)$ provided by the authors of these EBL models. These models are available via Web sites,[62] analytical approximations (as in, e.g., Stecker et al. 2006), published tables (as in, e.g., Franceschini et al. 2008), or via private communications (which is the case for, e.g., Salamon & Stecker 1998; Primack et al. 2005; Gilmore et al. 2009; Finke et al. 2010 for this work). Since the optical depth values are usually available in tabular form, for exact values of observed energy E and redshift z, a linear interpolation of $\tau(E, z)$ is used for arbitrary values of E and z in our calculations below.

The range of predictions by these EBL models is illustrated in Figure 1 as a function of observed γ-ray energy for sources at different redshifts. The universe is optically thin ($\tau_{\gamma\gamma} < 1$) to γ-rays with energy below $\simeq$10 GeV up to redshift $z \simeq 3$, independently of the model (see also Hartmann 2007). This is due to the rapid extinction of EBL photons shortward of the Lyman limit. Gamma rays below ∼10 GeV are not attenuated substantially because of faint far-UV and X-ray diffuse backgrounds.

The primary sources of HE extragalactic γ-rays are blazars and GRBs. Blazars are AGNs with relativistic plasma outflows (jets) directed along our line of sight. GRBs are associated with the core collapse of massive stars or might be caused by binary mergers of neutron stars or neutron star–black hole systems. Some GRBs produce beamed HE radiation similar to the case of blazars but lasting for a short period of time. GRBs have not been used to constrain EBL absorption during the pre-*Fermi* era mainly because of a lack of sensitivity to transient objects above 10 GeV. The sensitivity of EGRET decreased significantly above 10 GeV, and the field of view (FoV) of TeV instruments is small (typically 2°–4°) to catch the prompt phase where most of the HE emission occurs. The new energy window (10–300 GeV) accessible by *Fermi*, and the wide FoV of the LAT, makes GRBs interesting targets to constrain EBL absorption in this energy band.

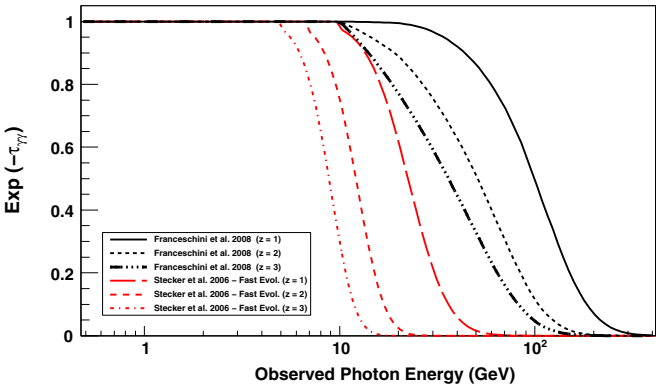

Figure 1. Attenuation as a function of observed gamma-ray energy for the EBL models of Franceschini et al. (2008) and Stecker et al. (2006). These models predict the minimum and maximum absorptions of all models in the literature and thus illustrate the range of optical depths predicted in the *Fermi*-LAT energy range.

(A color version of this figure is available in the online journal.)

Evaluating the ratio of the putatively absorbed to unabsorbed fluxes from a large number of distant blazars and GRBs observed by *Fermi* could result in interesting EBL constraints, as proposed by Chen et al. (2004), although intrinsic spectral curvature (e.g., Massaro et al. 2006) or redshift-dependent source internal absorption (Reimer 2007) could make this, or similar techniques, less effective. Georganopoulos et al. (2008) have proposed that Compton scattering of the EBL by the radio lobes of nearby radio galaxies such as Fornax A could be detectable by the *Fermi*-LAT. If identified as unambiguously originating from such process, a LAT detection of Fornax A could constrain the local EBL intensity.

Because the e-folding cutoff energy, $E(\tau_{\gamma\gamma} = 1)$, from $\gamma\gamma$ pair production in γ-ray source spectra decreases with redshift, modern Cherenkov γ-ray telescopes are limited to probing EBL absorption at low redshift due to their detection energy thresholds typically at or below 50 GeV–100 GeV (Hinton & Hofmann 2009). Ground-based γ-ray telescopes have detected 35 extragalactic sources to date,[63] mostly of the high-synchrotron-peaked (HSP) BL Lacertae objects type. The most distant sources seen from the ground with a confirmed redshift are the flat spectrum radio quasar (FSRQ) 3C 279 at $z = 0.536$ (Albert et al. 2008) and PKS 1510−089 at $z = 0.36$ (Wagner et al. 2010). Observations of the closest sources at multi-TeV energies have been effective in placing limits on the local EBL at mid-IR wavelengths, while spectra of more distant sources generally do not extend above 1 TeV, and therefore probe the optical and near-IR starlight peak of the intervening EBL (e.g., Stecker & de Jager 1993; Stanev & Franceschini 1998; Schroedter 2005; Aharonian et al. 1999, 2002; Costamante et al. 2004; Aharonian et al. 2006; Mazin & Raue 2007; Albert et al. 2008; Krennrich et al. 2008; Finke & Razzaque 2009).

The starting point for constraining the EBL intensity from observations of TeV γ-rays from distant blazars with atmospheric Cherenkov telescopes is the assumption of a reasonable intrinsic blazar spectrum, which, in the case of a power law, $dN/dE \propto E^{-\Gamma_{\rm int}}$, for example, is not harder than a pre-specified minimum value, e.g., $\Gamma_{\rm int} \geqslant \Gamma_{\rm min} = 0.67$ or 1.5. Upper limits (ULs) on the EBL intensity are obtained when the reconstructed intrinsic spectral index from the observed spectrum, $\Gamma_{\rm obs}$,

[62] http://www.physics.adelaide.edu.au/tkneiske/Tau_data.html for Kneiske et al. (2004); http://www.phy.ohiou.edu/finke/EBL/index.html for Finke et al. (2010).

[63] e.g., http://www.mpi-hd.mpg.de/hfm/HESS/pages/home/sources/, http://www.mppmu.mpg.de/rwagner/sources/

presumably softened by EBL absorption of very high energy (VHE) γ-rays, is required to not fall below $\Gamma_{\rm int}$. The minimum value of Γ has been a matter of much debate, being reasoned to be $\Gamma_{\rm int} = 1.5$ by Aharonian et al. (2006) from simple shock acceleration theory and from the observed spectral energy distribution (SED) properties of blazars, while Stecker et al. (2007) argued for harder values (less than 1.5) under specific conditions based on more detailed shock acceleration simulations. Katarzyński et al. (2006) suggested that a spectral index as hard as $\Gamma_{\rm int} = 0.67$ was possible in a single-zone leptonic model if the underlying electron spectrum responsible for inverse-Compton emission had a sharp lower-energy cutoff. Böttcher et al. (2008) noted that Compton scattering of the cosmic microwave background radiation by extended jets could lead to harder observed VHE γ-ray spectra, and Aharonian et al. (2008) have argued that internal absorption could, in some cases, lead to harder spectra in the TeV range as well.

A less model-dependent approach uses the (unabsorbed) photon index as measured in the sub-GeV range as the intrinsic spectral slope at GeV–TeV energies. This method has recently been applied to PG 1553+113 (Abdo et al. 2010a) and 1ES 1424+240 (Acciari et al. 2010; Prandini et al. 2010) to derive ULs on their uncertain redshifts, and to search for EBL-induced spectral softening in *Fermi* observations of a sample of a TeV-selected AGN (Abdo et al. 2010i).

Attenuation in the spectra of higher redshift objects ($z \gtrsim 1$) may be detectable at the lower energies that are accessible to the *Fermi*-LAT, i.e., at $E \approx$ 10–300 GeV. Gamma rays at these energies are attenuated mainly by the evolving UV background, which is produced primarily by young stellar populations and closely traces the global star formation rate. Observations with *Fermi* of sources out to high redshift could therefore reveal information about the star formation history of the universe, as well as the uncertain attenuation of UV starlight by dust.

In this paper, we present constraints on the EBL intensity of the universe derived from *Fermi*-LAT observations of blazars and GRBs. The highest energy γ-rays from high-redshift sources are the most effective probe of the EBL intensity, and consequently a powerful tool for investigating possible signatures of EBL absorption. In contrast to ground-based γ-ray detectors, *Fermi* offers the possibility of probing the EBL at high redshifts by the detection of the AGN at $\gtrsim$10 GeV energies out to $z > 3$, and additionally by the detection of GRB 080916C at a redshift of $\sim$4.35 (Abdo et al. 2009a; Greiner et al. 2009). GRBs are known to exist at even higher redshifts (GRB 090423 is the current record holder with $z \sim 8.2$; Tanvir et al. 2009). Therefore, observations of these sources with *Fermi* are promising candidates for probing the optical-UV EBL at high redshifts that are not currently accessible to ground-based (Cherenkov) telescopes.

In Section 2, we describe our data selections, the *Fermi*-LAT AGN and GRB observations during the first year of operation and analysis, and we discuss potential biases in the selection. Our methodology and results are presented in Section 3. We discuss implications of our results in Section 4 and conclude in Section 5.

In the following, energies are in the observer frame except where noted otherwise.

2. OBSERVATIONS AND DATA SELECTION

The *Fermi*-LAT is a pair-conversion detector sensitive to γ-rays with energies greater than 20 MeV. The LAT has a peak effective area $\geqslant$8000 cm^2 at energies greater than 1 GeV relevant for most of the event selections considered in this analysis and a large, $\sim$2.4 sr, FoV. The angular resolution for the 68% containment radius is $\sim 0.^\circ 6$ for 1 GeV photons that convert in the upper layers of the tracker (*front* events) and about a factor of two larger for those that convert in the bottom layers of the tracker (*back* events). A simple acceptance-averaged approximation for the 68% containment angle that is helpful to illustrate the energy-dependent point-spread function (PSF) is $\langle\theta_{68}(E)\rangle = (0.^\circ 8) \times (E/\mathrm{GeV})^{-0.8} \bigoplus (0.^\circ 07)$. A full description of the LAT instrument is reported in Atwood et al. (2009).

The data set used for the analysis of the AGNs includes LAT events with energy above 100 MeV that were collected between 2008 August 4 and 2009 July 4. LAT-detected GRBs are considered up to 2009 September 30. A zenith angle cut of 105° was applied in order to greatly reduce any contamination from the Earth albedo. Blazars and GRBs have different emission characteristics, which result in different analysis procedures here. The event rate detected by the LAT in the vicinity (68% confidence radius) of a blazar is largely background dominated and only continuous observations over long time scales allow the detection of the underlying blazar emission. To minimize the background contamination when analyzing blazar data we use the "diffuse" class events, which provide the purest γ-ray sample and the best angular resolution. GRBs, on the other hand, emit most of their radiative γ-ray power on very short time scales (typically on the order of seconds) where the event rate can be considered mostly background free (at least during the prompt emission of bright bursts). It is therefore possible to loosen the event class selection to increase the effective area at the expense of a higher background rate which is still small on short time scales for bright bursts. The "transient" class was designed for this specific purpose and we use these events for GRB analysis.[64]

2.1. AGN Sample and Potential Biases

We use blazars extracted from the First LAT AGN Catalog (1LAC; Abdo et al. 2010e) as the AGN source sample to probe the UV through optical EBL. This catalog contains 671 sources at high Galactic latitude ($|b| > 10^\circ$) associated with high confidence with blazars and other AGNs that were detected with a test statistic[65] TS > 25 during the first 11 months of science operation of the LAT. Detection of correlated multiwavelength variability was required in order to establish a source as being identified.

Source associations were made with a Bayesian approach (similar to Mattox et al. 2001). The Bayesian approach for source association implemented in the *gtsrcid* tool of the LAT *ScienceTools* package[66] uses only spatial coincidences between LAT and the counterpart sources. Candidate source catalogs used for this procedure include CRATES (Healey et al. 2007), CGRaBS (Healey et al. 2008) and the Roma-BZCAT (Massaro et al. 2009), which also provide optical classifications and the latter two provide also spectroscopic redshifts for the sources. See Abdo et al. (2010e) for further details on the source detection and association algorithms referred to here.

As discussed below, some methods applied here require one to distinguish among the different blazar source classes. FSRQs and BL Lac objects are discerned by their observed

[64] see Atwood et al. (2009) for further details on LAT event selection.

[65] The test statistic (TS) is defined as TS $= -2 \times (\log(L_0) - \log(L_1))$ with L_0 the likelihood of the Null-hypothesis model as compared to the likelihood of a competitive model, L_1, (see Section 3.2.2).

[66] http://fermi.gsfc.nasa.gov/ssc/data/analysis/scitools/overview.html

optical emission line equivalent widths and the Ca II break ratio (e.g., Stocke et al. 1991; Marcha et al. 1996) following the procedure outlined in Abdo et al. (2009b). The BL Lac object class itself is sub-divided into low-, intermediate-, and high-synchrotron-peaked BL Lac objects (denoted as LSP-BLs, ISP-BLs, and HSP-BLs, respectively) by estimating the position of their synchrotron peak, $\nu^s_{\rm peak}$, from the indices $\alpha_{\rm ox} \simeq 0.384 \cdot \log(f_{5000\rm A}/f_{1\ \rm keV})$ and $\alpha_{ro} \simeq 0.197 \cdot \log(f_{5\ \rm GHz}/f_{5000\rm A})$ determined by the (rest frame) optical ($f_{5000\rm A}$), X-ray ($f_{1\ \rm keV}$), and radio ($f_{5\ \rm GHz}$) flux densities listed in the online version of the Roma-BZCAT blazar catalog (Massaro et al. 2009), and using an empirical relationship between those broadband indices and $\nu^s_{\rm peak}$ as derived in Abdo et al. (2010d). LSP-BLs have their synchrotron peak at $\nu^s_{\rm peak} < 10^{14}$ Hz, ISP-BLs at 10^{14} Hz $\leqslant \nu^s_{\rm peak} \leqslant 10^{15}$ Hz, and HSP-BLs at $\nu^s_{\rm peak} > 10^{15}$ Hz. This is found to be in agreement with the classifications used in Abdo et al. (2010c, 2010d). Nearly all the 296 FSRQs are of LSP-type, while only 23% of the 300 BL Lac objects are LSP-BLs, 15% are ISP-BLs, and 39% are HSP-BLs, 72 AGNs could not be classified, and 41 AGNs are of other type than listed above.

Redshift information on the sources is extracted from the counterpart source catalogs (CRATES, CGRaBS, and Roma-BZCAT). While all the redshifts of the 1LAC FSRQs are known, only 42% of the high-confidence BL Lac objects have measured redshifts. Obviously, AGNs without redshift information are not used in the present work.

The intrinsic average photon indices of *Fermi* blazars in the LAT energy range indicate a systematic hardening with source type from ∼2.5 for FSRQs via ∼2.2 for LSP- and ∼2.1 for ISP-, to ∼1.9 for HSP-BLs (Abdo et al. 2010c). On the other hand, their redshift distributions systematically decrease from the high-redshift (up to $z \sim 3.1$) FSRQs, via LSP-BLs located up to a redshift $z \sim 1.5$, down to the mostly nearby HSP-BLs at $z < 0.5$. This mimics a spectral softening with redshift if blazars are not treated separately by source type. A search for any systematic spectral evolution must therefore differentiate between the various AGN sub-classes (see below).

To detect absorption features in the HE spectra (>10 GeV; see Figure 1) of *Fermi* blazars, a thorough understanding of their intrinsic spectra, including variability and source internal spectral features, is required. Most blazars do not show strong spectral variability in the LAT energy range on $\gtrsim$ week scales (Abdo et al. 2010c), despite often strong flux variability (Abdo et al. 2010g). Indeed at least three blazars, which turn out to constrain the UV EBL the most (see Sections 3.2.1 and 3.2.2), show a >99% probability of being variable in flux (using a χ^2 test) with a normalized excess variance of ∼0.02–0.2 on timescales of hours to weeks. PKS 1502+106 (J1504+1029) is one of the most constraining sources in the sample. It displayed an exceptional flare in 2008 August with a factor ∼3 increase in flux within ∼12 hr (Abdo et al. 2010b). During this flare a flatter (when brighter) spectral shape was evident. The spectral curvature at the HE end increased with decreasing flux level. If the HE ($\gtrsim$10 GeV) photons are emitted during such flare activity, the constraints on the γ-ray optical depth would be tighter if only the flare-state spectral data were used. Because of limited photon statistics during the flare, however, we use the more conservative time-averaged spectrum in the present analysis.

Absorption in radiation fields internal to the source (e.g., accretion disk radiation, photon emission from the broad line region) may cause a systematic break in the γ-ray spectra that coincidentally mimics EBL attenuation (Reimer 2007). In the case where such internal absorption occurs, its redshift dependence is guaranteed, even in the absence of accretion evolution. This is because of the redshifting of that energy where the interaction probability is maximum (Reimer 2007). Any technique that explores systematic variation of observables (e.g., changes in spectral slope, flux ratios, and *e*-folding cutoff energy) with redshift to single out EBL-induced absorption features in blazars with luminous accretion disk radiation (possibly indicated by strong emission lines) might therefore suffer from such a bias.

All bright strong-line *Fermi* blazars (i.e., *Fermi*-FSRQs and some LSP- and ISP-BLs), however, have been found to show spectral breaks already in the 1–10 GeV (source frame) range (Abdo et al. 2010c). This is too low in energy to be caused by EBL attenuation for their redshift range $\lesssim$3 (see Figure 1). Although it is not clear if these breaks are due to internal absorption, the spectral softening results in low photon counts at energies $\gtrsim$10 GeV where EBL absorption is expected. Spectra of all bright HSP-BLs and some ISP-BLs, on the other hand, can be well represented by simple power laws without any signs of curvature or breaks. This indicates not only do they not have significant internal absorption in the γ-ray band, but also the absence of significant EBL absorption, which is expected to be beyond the LAT energy range for this nearby ($z \lesssim 0.5$) blazar population.

Consequently, as we show in Section 3.1, it remains challenging to quantify EBL absorption effects in the LAT energy range based on population studies. On the other hand, the determination of the EBL-caused absorption features from individual blazars requires bright, high-redshift objects with spectra extending to $\gg$10 GeV (Figure 1), and we focus on these blazars in Section 3.2.

2.2. GRB Sample and Potential Biases

The *Fermi*-LAT has detected 11 GRBs from the beginning of its science operation (2008 August 4) until 2009 September 30, six of which have redshift measurements. Figure 3 shows the redshift and highest energy event associated with each of these GRBs. The probability of non-association is extremely small (see Table 1).

GRB prompt emission is highly variable and shows signs of spectral evolution, a source of systematics to be considered carefully. Our approach in this paper is to restrict ourselves to the analysis of small time windows during the GRB emission where the temporal behavior does not seem to change significantly.

The GRB spectral behavior is well represented by the Band function (Band et al. 1993) in the keV–MeV range. An additional hard, $\Gamma \sim 1.5$–2, power-law component, dominating at $\gtrsim$100 MeV, has now been firmly identified in a few GRBs: GRB090510 (Ackermann et al. 2010), GRB090902B, (Abdo et al. 2009c), and GRB090926A (Abdo et al. 2010j). Its absence in other LAT bursts could well be due to limited photon statistics. We assume that the power-law component extends well beyond 100 MeV up to ∼10 GeV, below which EBL absorption is negligible (see Figure 1). EBL absorption is then expected to soften the power-law spectra from the extrapolation of the intrinsic/unabsorbed spectra beyond ∼10 GeV. Systematic effects will, of course, occur when an intrinsic spectrum at high energies differs from this extrapolation. Source internal and/or intrinsic absorption via pair creation, e.g., would produce a

curvature of the spectrum at higher energy which could be misinterpreted as an EBL absorption effect. Such a spectral break, which could be due to intrinsic pair creation, was detected in the LAT data from GRB 090926A (Abdo et al. 2010j) but we note that a corresponding roll-off in the intrinsic spectrum can only make our limits on the γ-ray optical depth more conservative. By contrast, a rising spectral component above >10 GeV would make our limits less constraining, but in the absence of any evidence for inverted gamma-ray spectra in GRBs, we consider this possibility unlikely.

3. ANALYSIS OF γ-RAY FLUX ATTENUATION AND RESULTS

Assuming that HE photon absorption by the EBL is the sole mechanism that affects the γ-ray flux from a source at redshift z, the observed (i.e., absorbed) and unabsorbed fluxes at the observed energy E can be related by the optical depth, $\tau_{\gamma\gamma}(E, z)$, as

$$F_{\rm obs}(E) = \exp[-\tau_{\gamma\gamma}(E, z)]F_{\rm unabs}(E). \quad (1)$$

This is the primary expression that we use to (1) explore γ-ray flux attenuation in the EBL from AGNs by means of a redshift-dependent flux ratio between a low- and a HE band; (2) constrain EBL models which predict $\tau_{\gamma\gamma}(E, z)$ values much higher than the optical depth that would give the observed fluxes from individual blazars and GRBs; and (3) put ULs on the γ-ray optical depth calculated from the observed flux of individual blazars and GRBs, and the extrapolation of the unabsorbed flux to high energies. We discuss these methods and the results from our analysis below.

3.1. Flux Ratios—A Population-based Method

Because of inherent uncertainties in the determination of the intrinsic spectrum ($\Gamma_{\rm int}$) for any given blazar in the pre-*Fermi* era, Chen et al. (2004) proposed the average ratio $F(>10\ {\rm GeV})/F(>1\ {\rm GeV})$ for all blazars with significant detections above 1 GeV, weighted according to the errors in $F(>1\ {\rm GeV})$, as a redshift-dependent tracer of the EBL attenuation of γ-ray flux. The average flux ratio could then be compared with the predictions of the EBL models, taking selection effects into account. This approach assumes that the blazars are sampled from a homogeneous distribution with a single redshift-dependent luminosity function and a single intrinsic spectral index distribution. Preliminary results from *Fermi* (Abdo et al. 2009b) indicate that this assumption is inadequate. Consequently, we have calculated the average flux ratios for the different classes of blazars and discuss the results below.

Among the AGN sample described in Section 2.1, we find that 237 FSRQs, 110 BL Lac objects, and 25 other AGNs are clean[67] 1LAC associations with known redshift and detectable fluxes at energies $\geqslant$1 GeV. There are 30 LSP-, 18 ISP-, and 60 HSP-BL Lac objects in this sub-sample.

Of these AGN, only 22 FSRQs, 49 BL Lac objects, and 1 other AGN have flux detections rather than ULs above 10 GeV, including 10 LSP-, 6 ISP-, and 33 HSP-BL Lac objects. For each of these BL Lac objects and FSRQs, we calculated the ratio between the fluxes above 10 GeV and 1 GeV and their corresponding statistical errors following Chen et al. (2004).

[67] i.e., its association probability is at least 80%, it is the sole AGN associated with the corresponding γ-ray source, and it is not flagged to have problems that cast doubt on its detection (Abdo et al. 2010e).

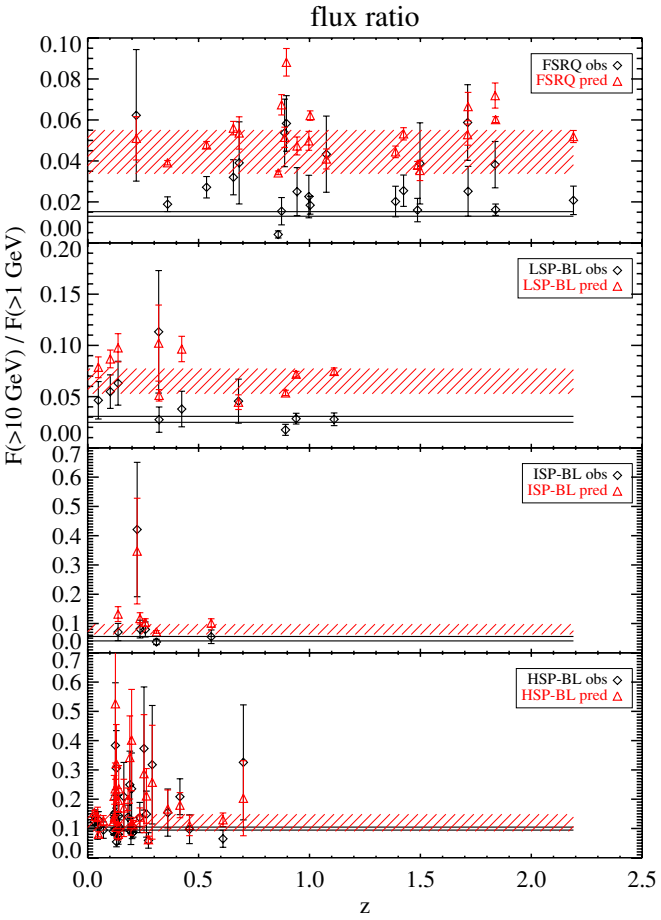

Figure 2. Flux ratio $F(\geqslant 10\ {\rm GeV})/F(\geqslant 1\ {\rm GeV})$ as a function of redshift, in the *Fermi*-LAT energy range, for FSRQs and BL Lac object populations. The black diamonds (filled circles in the printed journal) are the observed ratios, while the triangles show the ratio expected assuming an unbroken power law and no EBL attenuation. The black horizontal solid lines and cross-hatched regions correspond to the mean observed ratios and expected ratios with errors.

(A color version of this figure is available in the online journal.)

Figure 2 shows the observed flux ratios for the FSRQ population and BL Lac object sub-populations as well as the ratios predicted according to the 1FGL spectral index of each blazar, assuming an unbroken power law and no EBL attenuation. Table 1 shows the mean spectral index, mean flux ratios observed and expected, and the reduced χ^2 and associated probability given a parent distribution with constant flux ratio. As the blazar classes progress from FSRQ through LSP-BL, ISP-BL, and HSP-BL,

1. the range of redshifts becomes narrower;
2. on average, the spectra become harder;
3. both the predicted and observed mean flux ratios increase; and
4. the difference between the predicted and observed flux ratios decreases.

The trend in the predicted flux ratios is a direct consequence of the hardening of the spectra as a function of source class, while the difference between the predicted and observed flux ratios is due to the fact that the curvature of the spectra decreases as the HE peak of the SED moves through the *Fermi*-LAT energies. The apparent discrepancies between the flux ratios for different blazar sub-populations arise from the fact that the

Table 1
Spectral Indices, Mean Predicted and Observed Flux Ratios, and Reduced χ^2 and Probability for Blazar Sub-populations

Blazar Type	Num	Γ	Ratio (pred)	Mean Ratio (obs)	Red. χ^2	Prob
FSRQ	22	2.3 ± 0.1	0.04 ± 0.01	0.014 ± 0.001	4.38	1.8×10^{-10}
LSP-BL	10	2.2 ± 0.1	0.07 ± 0.01	0.028 ± 0.003	1.65	0.11
ISP-BL	6	2.1 ± 0.1	0.08 ± 0.02	0.048 ± 0.008	1.86	0.11
HSP-BL	33	1.9 ± 0.1	0.12 ± 0.03	0.100 ± 0.005	1.29	0.13

LAT samples different parts of the blazar SED for these subclasses. Indeed, a redshift distribution of the flux ratios for the combined blazar populations would show a strong, apparently decreasing trend, giving the appearance of an EBL absorption effect. When we separate the blazars into sub-populations, we find no significant redshift dependence of the flux ratios within each sub-population. The dearth of sources at high redshift and the large spread of spectral indices make it difficult to use the mean trend in the flux ratio as a function of redshift. To set ULs on the γ-ray optical depth, we need to rely on the spectra of individual blazars, despite the increased dependence on the blazar emission model this entails.

The flux ratio versus redshift relationship for BL Lac objects is therefore primarily due to the differing intrinsic spectral characteristics of BL Lac objects, rather than from EBL absorption. This test is a reminder of the importance of a careful consideration of the intrinsic spectral characteristics of the source populations chosen to probe EBL absorption.

3.2. Constraints on EBL Models from Individual Source Spectra

The sensitivity of the LAT over a broad energy range provides a unique opportunity to probe γ-ray spectra from AGNs and GRBs at <10 GeV where EBL absorption is negligible and at $\gtrsim$10 GeV where EBL absorption can be substantial (see Figure 1). Thus, extrapolations of the unabsorbed flux at low energies from individual sources to high energies, and assuming that the intrinsic spectra do not become harder at high energies, allows us to derive a measure of the total absorption (source in situ and in EBL). We note that this is the only assumption made for the following methods. Furthermore, since any intrinsic spectral curvature or internal absorption effects cannot be decoupled from EBL-caused curvature, the constraints derived below shall be considered as conservative ULs on the EBL-caused opacity. These are then confronted with various EBL models. Clearly, high EBL density models possess a higher probability of being constrained by these methods than low density ones. In the following, we use two methods: the highest energy photon (HEP; Section 3.2.1) and the likelihood (Section 3.2.2) methods.

3.2.1. Highest Energy Photons

A simple method to constrain a given EBL model is to calculate the chance probability of detecting a photon with energy $E \geqslant E_{\rm max}$, where $E_{\rm max}$ is the energy of the most energetic photon that we would expect when the source intrinsic spectrum is folded with the optical depth from the specific EBL model we want to test. We derive a conservative estimate of the intrinsic flux of the source by extrapolating the unabsorbed spectrum at low energies to high energies. We consider the LAT spectrum to be representative of the intrinsic spectrum at energies where the EBL is supposed to absorb less than ∼1% of the photons for the most opaque models. This corresponds to an energy of around 10 GeV (down to ∼6 GeV for GRB 080916C at $z \sim 4.3$).

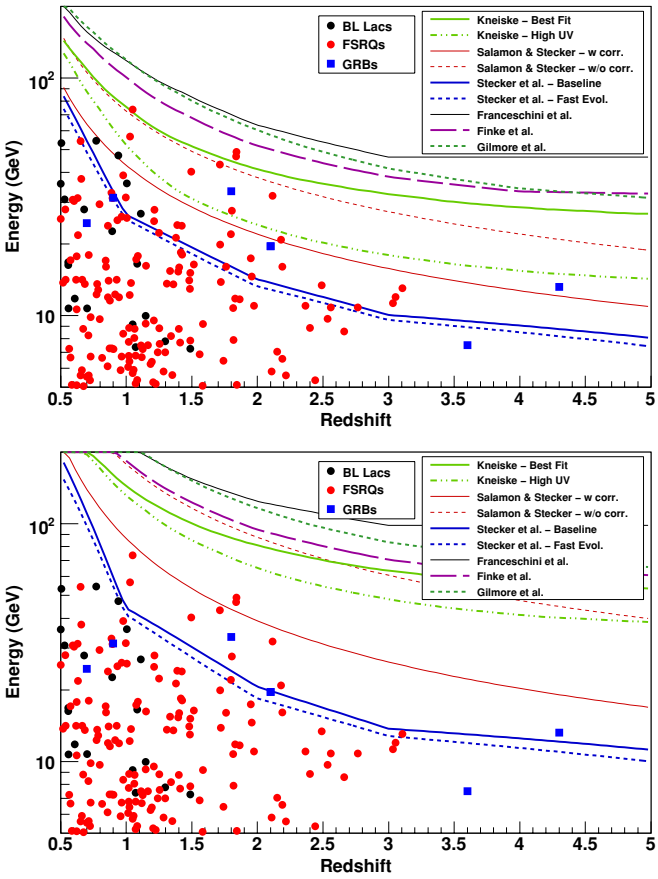

Figure 3. Highest energy photons from blazars and GRBs from different redshifts. Predictions of $\gamma\gamma$ optical depth $\tau_{\gamma\gamma} = 1$ (top panel) and $\tau_{\gamma\gamma} = 3$ (bottom panel) from various EBL models are indicated by lines. Photons above model predictions in this figure traverse an EBL medium with a high γ-ray opacity. The likelihood of detecting such photon considering the spectral characteristics of the source are considered in the method presented in Section 3.2.1.

Best-fit spectral parameters of this "low-energy" unabsorbed spectrum were derived for all sources of the HEP set (see Table 3). The spectrum is assumed to be a power law unless a significant deviation from this shape is measured at $\lesssim$10 GeV (as is indeed observed from, e.g., FSRQs at GeV energies). This is the case for source J1504+1029 for which a log-parabola model provides the best fit.

Iterating through the source list described in Sections 2.1 and 2.2 we find the energy $E_{\rm max}$ of the HEP detected within the 68% containment radius (using the specific P6_V3_DIFFUSE instrument response functions for front and back events) of each source position. The resulting $E_{\rm max}$ versus source redshift is shown in Figure 3 for sources with $z > 0.5$, and compared to the energy at which the optical depth $\tau_{\gamma\gamma}$ is equal to 1 and 3 according to the various EBL models. As shown in this figure, five AGNs have $E_{\rm max}$ that is significantly greater ($\gtrsim$2) than the energy at which $\tau_{\gamma\gamma} = 3$ for the "baseline EBL model" of

Table 2
List of Blazars and GRBs Detected by LAT which have Redshift Measurements, and which Constrain the EBL Opacity the Most

Source	z	$E_{\rm max}$ (GeV)	Conv. Type	$\Delta E/E$	68% Radius	Separation	Chance Probability
J1147−3812 (PKS 1144−379)	1.05	73.7	Front	10.7%	0.°054	0.°020	7.0×10^{-4}
J1504+1029 (PKS 1502+106)	1.84	48.9	Back	5.4%	0.°114	0.°087	5.6×10^{-3}
		35.1	Back	12.4%	0.°117	0.°086	9.8×10^{-3}
		23.2	Front	7.2%	0.°072	0.°052	5.6×10^{-3}
J0808−0751 (PKS 0805−07)	1.84	46.8	Front	9.7%	0.°057	0.°020	1.5×10^{-3}
		33.1	Front	5.9%	0.°063	0.°038	2.7×10^{-3}
		20.6	Front	8.9%	0.°075	0.°029	6.9×10^{-3}
J1016+0513 (CRATES J1016+0513)	1.71	43.3	Front	11.4%	0.°054	0.°017	1.2×10^{-3}
		16.8	Front	6.3%	0.°087	0.°035	8.2×10^{-3}
		16.1	Front	7.6%	0.°084	0.°018	8.2×10^{-3}
J0229−3643 (PKS 0227−369)	2.11	31.9	Front	10.7%	0.°060	0.°035	1.7×10^{-3}
GRB 090902B	1.82	33.4	Back	10.5%	0.°117	0.°077	6.0×10^{-8}
GRB 080916C	4.24	13.2	Back	11.6%	0.°175	0.°087	2.0×10^{-6}

Notes. For each source, J2000 coordinate based name (other name), the energy of the highest energy photon (HEP), the conversion type of the event (front or back) of the instrument, the energy resolution, $\Delta E/E$, for 68% containment of the reconstructed incoming photon energy, and the 68% containment radius based on the energy and incoming direction in instrument coordinates of the event, the separation from the source and the chance probability of the HEP being from the galactic diffuse or isotropic backgrounds are also listed. The energy resolution for the GRB HEP events is taken from Abdo et al. (2009c) and Abdo et al. (2009a) using the respective lower energy bounds. The three HEPs are listed for those sources that have multiple constraining photons.

Stecker et al. (2006). These five AGNs (and two comparable GRBs) have emitted a number of events (hereafter highest energy photons or HEP) that populate a region of the $E_{\rm max}$–z phase space where EBL attenuation effects are predicted to be significant. These (henceforth called "HEP set") will be used in the following sections to constrain EBL models and to calculate the maximum amount of EBL attenuation that is consistent with the LAT observations.[68]

It is possible that the HE photons considered here may not be emitted in the high-redshift source and instead originated in any of the following background sources: Galactic γ-ray diffuse, isotropic (extragalactic γ-ray + charged-particle residuals), or a nearby point source. The likelihood of detecting any of these background photons within the 68% containment radius used to find the HEP set is quantified by computing the number of expected events within the 68% containment radius at the location of the source as determined by the best-fit background model (Galactic and isotropic diffuse + point sources) and the instrument acceptance. The last column of Table 2 shows such probability for photons in the HEP set. These chance probabilities, although being fairly small, are non-negligible (at least in the case of blazars) if one would like to set significant constraints on specific EBL models by using this HEP. We later describe how this probability for the HEP to be a background fluctuation was incorporated in our final results for this method. For now we will assume that this HEP is indeed from the source and we will first derive the type of constraints it allows us to set on different EBL models. We also note that a stricter set of cuts (*extradiffuse*) has been developed by the LAT team to study the extragalactic γ-ray background (Abdo et al. 2010f). Despite the decreased γ-ray acceptance we find all photons in the HEP set to be retained when using these selection cuts.

[68] Only the highest energy photon from each source is shown in Figure 3. There are a few sources, however, with more than one constraining photon as indicated in Table 2.

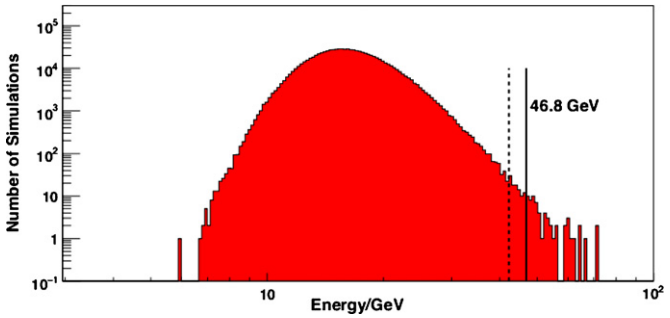

Figure 4. Distribution of highest energy photons obtained from Monte Carlo simulations of the source J0808−0751 with the EBL attenuation by Stecker et al. (2006). $E_{\rm max}$ and $E_{\rm max} - \sigma_{\rm Emax}$ (where $\sigma_{\rm Emax}$ is the energy uncertainty) are indicated by a solid and dotted vertical black lines, respectively. The probability of detecting a photon with energy equal or greater to $E_{\rm max} - \sigma_{\rm Emax}$ is equal to 6.8×10^{-5}.

(A color version of this figure is available in the online journal.)

Monte Carlo simulations are performed in order to test a particular EBL model with the derived intrinsic spectrum absorbed by the EBL as the Null hypothesis. The simulations were performed using *gtobssim*, one of the science tools distributed by the *Fermi* science supports center and the LAT instrument team. For each simulation, we define the unabsorbed spectrum of the source as a power law (or log parabola in the case of J1504+1029) with spectral parameters drawn randomly from the best-fit values (and corresponding uncertainty) shown in Table 3. EBL absorption is applied according to the optical depth values of the considered model, and finally, the position and orientation of the *Fermi* satellite during the time interval described in Section 2 is used to account for the instrument acceptance that corresponds to the observations. The HEP from the simulated data is obtained following the exact same cuts and analysis procedure that was used for the data.

The resulting distribution of the HEP simulated in each case (see, e.g., Figure 4) is used to estimate the chance probability of

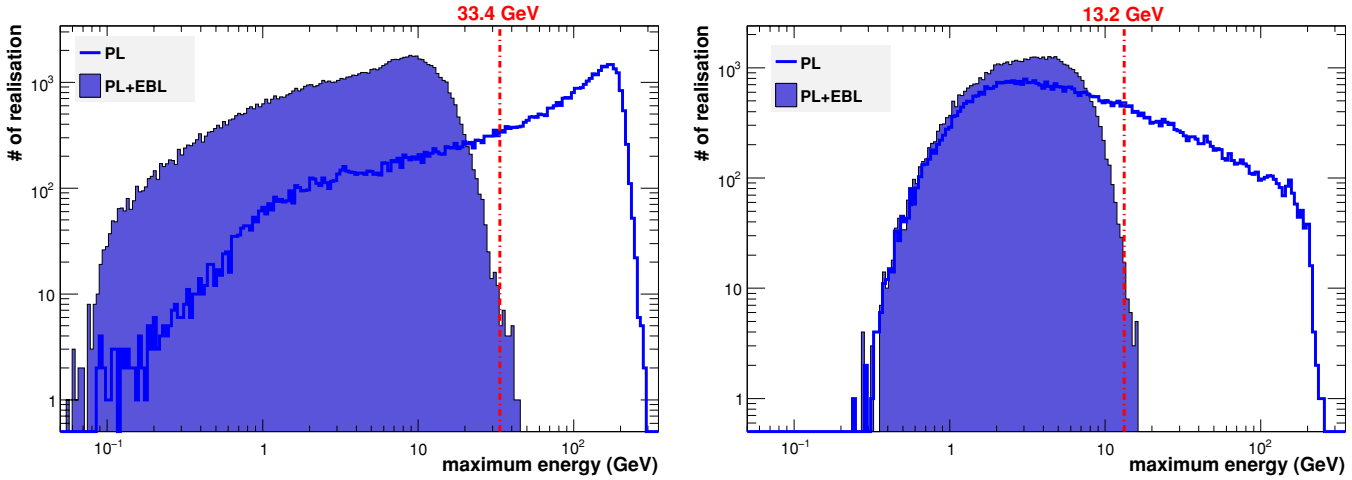

Figure 5. Distributions of the highest energy photons from simulations performed with estimates of our intrinsic spectra for GRB 080916C (left panel) and GRB 090902B (right panel), folded with EBL attenuation calculated using the Stecker et al. (2006) baseline model. The total number of realizations (10^5) in both the power law and power law convolved with the EBL cases is the same.

(A color version of this figure is available in the online journal.)

Table 3

Parameter Values of the Power-law (PL) Fits $dN/dE = N_0(-\Gamma+1)E^{-\Gamma}/[E_{\rm max}^{-\Gamma+1} - E_{\rm min}^{-\Gamma+1}]$ in the Range $E_{\rm min} = 100$ MeV to $E_{\rm max} = 10$ GeV of the Sources (AGNs and GRBs) Listed in Table 4, Except for Source J1504+1029 where a Log-parabolic Parameterization (LP) $dN/dE = N_0(E/E_b)^{-(\Gamma+\beta\log(E/E_b))}$ has been Found to be Preferable over a Power-law Fit (with ΔTS = 71.9)

Source	Normalization N_0 (10^{-7}ph cm^{-2} s^{-1} MeV^{-1})	Photon Index Γ (PL)	Γ, β, E_b/GeV (LP)	TS
J1147−3812	0.570 ± 0.081	2.38 ± 0.09	...	221
J1504+1029	(1.84 ± 0.23) × 10^{-4}	...	2.36 ± 0.03, 0.09 ± 0.01, 2.0 ± 0.1	34638
J0808−0751	1.212 ± 0.078	2.09 ± 0.04	...	1498
J1016+0513	1.183 ± 0.078	2.27 ± 0.05	...	1220
J0229−3643	0.789 ± 0.075	2.56 ± 0.07	...	394
J1012+2439	0.552 ± 0.058	2.21 ± 0.07	...	443
GRB 090902B	146 ± 56	1.40 ± 0.37	...	1956
GRB 080916C	1146 ± 199	2.15 ± 0.22	...	1398

Notes. The spectral fits for the GRBs are performed below 6 GeV and 3 GeV for GRB 090902B and GRB 080916C, respectively. The TS values are obtained through a likelihood-ratio test comparing a model with background only and a model where a point source was added.

detecting a photon from the source with energy equal or greater than $E_{\rm max}$. We produced ∼800,000 and ∼100,000 simulations for each of the HEP sets for AGN and for GRBs, respectively. Assuming the HEP is indeed from the source, the probability of observing such HE photon given the specific EBL model tested (called $P_{\rm HEP}$) is calculated as the ratio between the number of cases where the HEP energy is above $E_{\rm max}$ (actually $E_{\rm max}-\sigma_{\rm Emax}$ given the energy dispersion) and the total number of simulations performed. The number of simulations in each case was chosen to reach sufficient statistics at the tail of the distribution where the energy of the HEP is measured. Distributions of the HEP events from these MC simulations for GRB 080916C and GRB 090902B are shown in Figure 5. The open and filled histograms correspond to the distributions using the GRB spectra without and with EBL absorption using the "baseline model" of Stecker et al. (2006).

To compute the final probability of rejection for the specific EBL model tested (called $P_{\rm rejection}$), one needs to consider the fact that the HEP could be a background photon. We compute the probability for this to happen in Table 2 ($P_{\rm bkg}$). In the end, one can fail to reject the EBL model because the HEP might be a background event or because there is a chance for a source photon with energy $E_{\rm max}$ not to be absorbed by the EBL so that

$$P_{\rm rejection} = P_{\rm bkg} + P_{\rm HEP} \times (1 - P_{\rm bkg}). \quad (2)$$

In Table 4, we list these three probabilities for each of our most constraining sources. When more than one photon is available for a given source, the probabilities are combined resulting in a stronger rejection. Although $P_{\rm HEP}$ can be quite constraining, our final significance of rejection is limited by $P_{\rm bkg}$ which is non-negligible in the case of blazars and which depends on the size of the region around each source defined a priori to look for associated HE events (68% PSF containment radius in this analysis). A larger HEP acceptance region (90% or 95% containment radius instead of 68%) would increase the background

Table 4
Listed are the Significance of Rejecting the "Baseline" Model (Stecker et al. 2006), Calculated Using the HEP Method Described in Section 3.2.1

Source	z	Energy (GeV)	$P_{\rm bkg}$	HEP Method Applied to Stecker 06		HEP Rejection
				$P_{\rm HEP}$	$P_{\rm rejection}$	Significance
J1147−3812	1.05	73.7	7.0×10^{-4}	1.2×10^{-4}	8.1×10^{-4}	3.2σ
J1504+1029	1.84	48.9	5.6×10^{-3}	6.7×10^{-5}	5.7×10^{-3}	
		35.1	9.8×10^{-3}	6.8×10^{-3}	1.7×10^{-2}	
		23.2	5.6×10^{-3}	1.8×10^{-1}	1.9×10^{-1}	
				Combined $P_{\rm rej} = 1.7 \times 10^{-5}$		4.1σ
J0808−0751	1.84	46.8	1.5×10^{-3}	1.9×10^{-4}	1.7×10^{-3}	
		33.1	2.7×10^{-3}	3.7×10^{-3}	6.4×10^{-3}	
		20.6	6.9×10^{-3}	2.5×10^{-1}	2.6×10^{-1}	
				Combined $P_{\rm rej} = 2.8 \times 10^{-6}$		4.5σ
J1016+0513	1.71	43.3	1.1×10^{-3}	5.4×10^{-4}	1.6×10^{-3}	
		16.8	8.2×10^{-3}	4.9×10^{-1}	4.9×10^{-1}	
		16.1	8.2×10^{-3}	6.5×10^{-1}	6.5×10^{-1}	
				Combined $P_{\rm rej} = 5.3 \times 10^{-4}$		3.3σ
J0229−3643	2.11	31.9	1.7×10^{-3}	8.9×10^{-5}	1.8×10^{-3}	2.9σ
GRB 090902B	1.82	33.4	2×10^{-6}	2.0×10^{-4}	2.0×10^{-4}	3.7σ
GRB 080916C	4.24	13.2	8×10^{-8}	6.5×10^{-4}	6.5×10^{-4}	3.4σ

Notes. For completeness, we also report individually the probability of the HEP to be a background event ($P_{\rm bkg}$) and the probability for this HEP not to be absorbed by the EBL if it were emitted by the source ($P_{\rm HEP}$) following Equation (2). For those sources with more than one constraining photon, the individual and combined $P_{\rm rejection}$ are calculated. The "fast evolution" model by Stecker et al. (2006) is more opaque and leads to an even higher significance of rejection. Applying this method to less opaque models leads to no hints of rejection since the probability $P_{\rm HEP}$ is large in those cases (e.g., $\gtrsim$0.1 for the Franceschini et al. 2008 EBL model). Note that a log-parabola model was used as the intrinsic model for source J1504+1029 since evidence of curvature is observed here even below 10 GeV (see Table 3).

probability $P_{\rm bkg}$ while also adding constraining photons to the HEP set. On a source-by-source basis, the rejection probability goes up or down with increasing radius depending on the number and energy of these additional photons, but our overall result remains the same. The unbinned likelihood method, which we describe in the next Section (3.2.2), does not make use of an acceptance radius, and instead makes full use of available information in the data to systematically calculate a model rejection probability.

The analysis described in this section was applied to all sources from the HEP set. We find the "baseline" model of Stecker et al. (2006) to be significantly constrained by our observations. Column 5 of Table 5 shows the optical depth of the "baseline" model of Stecker et al. (2006) for the HEP events. Since the "fast-evolution" model[69] of Stecker et al. (2006) predicts higher opacities in the LAT energy range at all redshifts, our constraints on this model will naturally be higher than the ones found in Table 5 for the "baseline" model.

3.2.2. Likelihood Method

This second method to constrain specific EBL models makes use of a likelihood ratio test (LRT) technique. This approach compares the likelihood of the Null-hypothesis model (L_0) to best represent the data with the likelihood of a competitive model (L_1). The test statistic (TS) is defined as TS $= -2 \times (\log(L_0) - \log(L_1))$. Following Wilks' theorem (Wilks 1938), the TS is asymptotically distributed as χ^2_n (with n being the difference in degrees of freedom between the two models) if the two models under consideration satisfy the following two conditions (Protassov et al. 2002): (1) the models must be nested and (2) the null values of the additional parameters are not on the boundary of the set of possible parameter values.

For the LRT, we use the power-law intrinsic spectrum convolved with the EBL absorption predicted by the model ($\tau_{\rm mod}$) we are testing, $\exp[-\alpha\tau_{\rm mod}(E, z)]F_{\rm unabs}(E)$, as the observed flux. For the Null hypothesis, we set $\alpha = 1$ and we compare it to an alternative model where α is left as a free parameter, which therefore has one more degree of freedom than the Null hypothesis. In the absence of any flux attenuation by the EBL, $\alpha = 0$. Note that we allow the normalization parameter, α to go to negative values. This choice, although not physically motivated, allows us to satisfy the second condition mentioned above. As a consequence the TS can simply be converted into a

Table 5
Gamma-ray Optical Depth to HEP Calculated Using the EBL Model of Franceschini et al. (2008, F08) in Comparison with the "Baseline" Model of Stecker et al. (2006, St06)

Source	z	$E_{\rm max}$ (GeV)	$\tau(z, E_{\rm max})$ (F08)	$\tau(z, E_{\rm max})$ (St06, Baseline)	Number of Photons Above 15 GeV
J1147 −3812	1.05	73.7	0.40	7.1	1
J1504+1029	1.84	48.9	0.56	12.2	7
J0808−0751	1.84	46.8	0.52	11.7	6
J1016+0513	1.71	43.3	0.39	9.0	3
J0229−3643	2.11	31.9	0.38	10.2	1
GRB 090902B	1.82	33.4	0.28	7.7	1
GRB 080916C	4.24	13.2	0.08	5.0	1

Notes. Also listed are the number of photons associated with the source which have $\geqslant$15 GeV energy and which can potentially constrain EBL models.

[69] The "baseline" model considers the case where all galaxy 60μm luminosities evolved as $(1+z)^{3.1}$ up to $z \leqslant 1.4$, non-evolving between $1.4 < z < 6$ and no emission at $z > 6$. In contrast, the "fast-evolution" model assumes a more rapid galaxy luminosity evolution: $\propto (1+z)^4$ for $z < 0.8$, $\propto (1+z)^2$ for $0.8 < z < 1.5$, no evolution for $1.5 < z < 6$, and no emission at $z > 6$. Consequently, for a given redshift the "fast-evolution" model predicts a higher γ-ray attenuation than the "baseline" model.

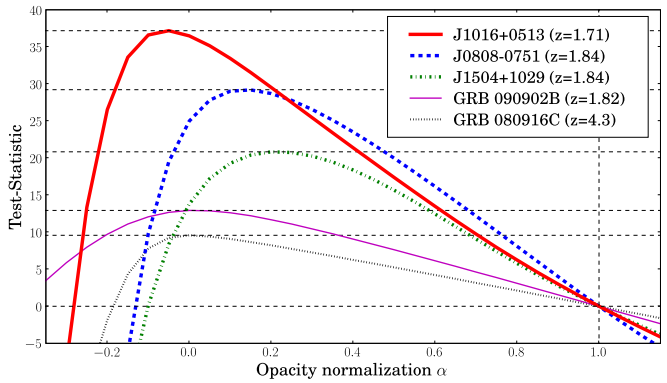

Figure 6. Test statistic (TS) as a function of the γ-ray optical depth normalization parameter calculated from the likelihood ratio test (LRT) for J1016+0513, J0808−0751, J1504+1029, and GRBs 090902B and 080916C. The "baseline" model of Stecker et al. (2006) has been used and the rejection for this model can be directly read out as ΔTS between $\alpha = 1$ and the best-fit α for the source (horizontal dashed line). The confidence interval for the normalization parameter can be obtained using $\Delta\mathrm{TS} = \mathrm{CL}^2$ where CL is the confidence level. (A color version of this figure is available in the online journal.)

significance of rejecting the Null hypothesis by making use of Wilks' theorem. Because of the lack of information on the intrinsic spectrum of a distant source above 10 GeV, we use the (unabsorbed) $\leqslant$10 GeV observed spectrum as a reasonable assumption for the functional shape of the intrinsic source spectrum. A simple power law was found to be a good fit to the $\leqslant$10 GeV data for the sources listed in Table 5 except in the case of J1504+1029 where a log-parabolic spectrum was preferred. We note that if the actual intrinsic curvature is more pronounced than the one found with the best fit below 10 GeV, this would only make the results more constraining.

As we mentioned earlier, although we are considering all EBL models in the literature, we find that our observations are only constraining the most opaque ones. Figure 6 shows the TS value as a function of the optical depth normalization parameter α, for the three most constraining blazars (J1016+0513, J0808−0751, and J1504+1029) and the two GRBs (GRBs 090902B and 080916C) when considering the "baseline" model of Stecker et al. 2006 with the LRT method. All sources are found to have an optical depth normalization parameter that is consistent with $\alpha \geqslant 0$ at the 1σ level which is reassuring as we do not expect a rise in the spectrum on a physical basis. $\sqrt{T S_{\max}}$ for $\alpha = 1$ corresponds to the rejection significance for the specific model considered. The most constraining source, J1016+0513, rejects the Null hypothesis ($\alpha = 1$, corresponding to the "baseline" model of Stecker et al. 2006 in this case) with a significance of $\sim 6.0\sigma$. This source could also constrain the "high UV model" of Kneiske et al. (2004) with a significance of 3.2σ although multi-trials effect substantially reduce this significance (see Section 3.2.3).

As compared to the HEP method, the LRT method incorporates the possibility of each photon being from the background into the unbinned maximum likelihood computation. Thus, separate calculations of the background probability and corresponding rejection probability are not needed. Also since the LRT method takes into account all HE photons rather than the highest energy ones in the HEP method, it gives more constraining results for the EBL model rejection with the exception of 2 GRBs where the HEP method gives slightly more constraining results. Finally, we note that the a priori choice of the size of the region around each source defined to look for associated HE events is a source of systematics for the HEP method (which uses 68% PSF containment radius) while it does not affect the LRT method.

Table 6
Significance of Rejecting the "Baseline" Model (Stecker et al. 2006), Calculated Using the LRT Method Described in Section 3.2.2

Source	z	LRT Rejection Significance	
		Pre-trial	Post-trial
J1147−3812	1.05	3.7σ	2.0σ
J1504+1029	1.84	4.6σ	3.3σ
J0808−0751	1.84	5.4σ	4.4σ
J1016+0513	1.71	6.0σ	5.1σ
J0229−3643	2.11	3.2σ	1.2σ
GRB 090902B	1.82	3.6σ	1.9σ
GRB 080916C	4.24	3.1σ	1.0σ

Notes. Again, the "fast-evolution" model by Stecker et al. (2006) leads to a high rejection significance with two sources (J0808− 0751 and J1016+0513) with $>4\sigma$ post-trial significance. The post-trial significance is computed by taking into account the fact that our analysis is considering ~200 independent sources.

3.2.3. Multi-trial Effects and Combined Probabilities

Because the search for EBL signatures or rejection of specific EBL models is performed on all blazars and GRBs detected by the LAT, one has to consider multi-trials, which is potentially affecting our analysis. For independent searches, as is the case here, the post-trial probability threshold for obtaining a 4σ result is $P_{\mathrm{post-trial}} = 1 - (1 - P_{4\sigma})^{1/N_{\mathrm{trials}}}$, where N_{trials} is the number of trials and $P_{4\sigma}$ is the 4σ probability threshold for a single search ($\approx 6.3 \times 10^{-5}$). In the present case, the LAT AGN catalog that we have used (Abdo et al. 2010e) includes 709 AGNs of which ~200 have a sufficiently high redshift (~100 with $\gtrsim$10 GeV photon) to allow for the testing of EBL attenuation models with their γ-ray spectra. Only a handful of LAT GRBs were observed with sufficient statistics to hope to constrain the EBL. In the end, we have $N_{\mathrm{trials}} \sim 200$ which corresponds to a post-trial probability for a 4σ result of $P_{4\sigma,\mathrm{post\text{-}trial}} \approx 3.17 \times 10^{-7}$. This corresponds to a significance of $\approx 5.11\sigma$ on an individual source which we will therefore consider as our threshold for a 4σ post-trials rejection significance for any specific EBL model. This $P_{4\sigma,\mathrm{post\text{-}trial}}$ threshold was reached in case of the Stecker et al. (2006) "baseline" model for sources J0808−0751 and J1016+0513 using the LRT method (see Table 6). Note that J1504+1029 is only slightly below this threshold.

Combining specific EBL model rejection probabilities from multiple sources[70] we get a much higher rejection significance. For HEP probabilities, the combined rejection significance for the Stecker et al. (2006) "baseline" model is $\approx 8.9\sigma$ ($\approx 7.7\sigma$ without the two GRBs) using Fisher's method in order to combine results from independent tests of the same Null hypothesis (Fisher 1925). For the LRT method, we add the individual likelihood profiles to derive an overall profile from which $\sqrt{\mathrm{TS}_{\max}}$ gives an overall significance of 11.4σ for the same EBL model. Therefore, both methods give very large rejection significances even after taking multi-trial effects into account. Since the Stecker et al. (2006) "fast-evolution" model gives opacities larger than the "baseline model" in the LAT

[70] Since the spectral fits of all the sources we considered in this analysis are independent to each other.

range, both models can be rejected by our analysis with very high confidence level. All other models cannot be significantly rejected even after such stacking procedure is applied.

3.3. Opacity Upper Limits

ULs on the γ-ray optical depth have been evaluated with a method based on the comparison between the measured energy spectrum of the source and the unabsorbed spectrum above 10 GeV. The unabsorbed spectrum, $F_{\rm unabs}$, is assumed to be the extrapolation of the low-energy part, $E < 10$ GeV, of the spectrum ($F_{E<10}$), where EBL attenuation is negligible (see Figure 1), to higher energies. $F_{E<10}$ is fitted with a power-law or log-parabola function, according to the best TS value. At high energies, if no intrinsic hardening of the spectrum is present, the measured spectrum, $F_{\rm obs}$, at (observed) energy E and the unabsorbed spectrum, $F_{\rm unabs}$, are related by Equation (1). The γ-ray optical depth can therefore be estimated at any given energy as

$$\tau_{\gamma\gamma}(E, z) = \ln[F_{\rm unabs}(E)/F_{\rm obs}(E)]. \quad (3)$$

Since $F_{\rm unabs}$ is evaluated assuming no EBL attenuation, it gives a maximum value. Therefore, the optical depth, $\tau_{\gamma\gamma}(E, z)$ given by Equation (3) could already be considered as a UL, assuming that the difference between $F_{\rm unabs}(E)$ and $F_{\rm obs}(E)$ is only due to EBL effects. The fit of both $F_{\rm obs}$ and $F_{E<10}$ are carried out with a maximum likelihood analysis (Mattox et al. 1996).[71]

To evaluate $F_{E<10}$, we have assumed a background model including all the point-like sources within 15° from the source under study and two diffuse components (Galactic and extragalactic). The Galactic diffuse emission is modeled using a *mapcube* function, while a tabulated model is used for the isotropic component, representing the extragalactic emission as well as the residual instrumental background.[72] Both diffuse components are assigned a free normalization for the likelihood fit. In the fit we have considered all the nearby point sources within a 10° radius, modeled with a power law with the photon index fixed to the value taken from the 1FGL catalog (Abdo et al. 2010h), and the integral flux parameter left free. The remaining point sources are modeled with a power law with all spectral parameters fixed.

The source under study has been fitted with a power law and a log parabola with all spectral parameters free. Among the two, we have chosen the fitted function showing the best TS value. The result is that for all the sources except J1504+1029 a power-law fit is preferred. From the fit results of $F_{E<10}$ we have extrapolated the spectral shape to obtain $F_{\rm unabs}(E)$ above 10 GeV.

A different method has been used to derive the measured flux $F_{\rm obs}$ in selected energy bins. The whole energy range from 100 MeV to 100 GeV is divided in equal logarithmically spaced bins requiring in each energy bin a TS value greater than 10:2 bins per decade above 10 GeV for J0229-3643, J1016+0513, and J1147-3812, 4 bins per decade for J0808−0750 and 5 bins per decade for J1504+1029. In each energy bin, the standard *gtlike* tool has been applied assuming for all the point-like sources a simple power-law spectrum with photon index fixed to 2.0.[73] The integral fluxes of all point-like sources within 10° are left as free parameters in the fitting procedure, while the diffuse background components are modeled as described in the previous paragraph. In this way, assuming that in each energy bin the spectral shape can be approximated with a power law, the flux of the source in all selected energy bins is evaluated.

Once both $F_{\rm unabs}$ and $F_{\rm obs}$ are determined, the maximum γ-ray optical depth in each energy bin can be estimated from Equation (3). A UL on $\tau_{\gamma\gamma}(\langle E\rangle, z)$ with 95% CL in a constraining energy bin with mean energy $\langle E\rangle$ is then calculated by propagating the parameter uncertainties in the fitted flux[74]:

$$\tau_{\gamma\gamma,{\rm UL}_{95\%}{\rm CL}}(\langle E\rangle, z) = \ln[F_{\rm unabs}(\langle E\rangle)/F_{\rm obs}(\langle E\rangle)] + 2\sigma. \quad (4)$$

We compare these limits with the γ-ray optical depths predicted by various EBL models.

In Figure 7, we show the ULs (95% CL) derived at the mean energy of the bins above 10 GeV for various objects. In the highest energy bin, the optical depth UL has been evaluated at the highest photon energy as reported in Table 4. At this energy, the results of the optical depth UL at 99% CL are also reported (blue arrow, thick black arrow in the print edition). As an example, consider blazar J0808−0751 at $z = 1.84$ shown in the upper left plot: a larger optical depth would require an intrinsic spectrum that at high energies lies significantly above the extrapolation obtained from the low energy spectrum. The figure shows that the UL rules out those EBL models that predict strong attenuation. This result is consistent with all other ULs derived with this method (see the other plots in Figure 7 and summary of the results in Table 7).

Table 7
Upper Limits (95% CL) on the γ-ray Optical Depth for AGNs in Table 4

Source	z	$E_{\rm max}$	$\tau_{\rm UL}(z, E_{\rm max})$	Energy Bins 10 GeV–100 GeV
J1147−3812	1.05	73.7	1.33	2 bins/dec
J1504+1029	1.84	48.9	1.82	5 bins/dec
J0808−0751	1.84	46.8	2.03	4 bins/dec
J1016+0513	1.71	43.3	0.83	2 bins/dec
J0229−3643	2.11	31.9	0.97	2 bins/dec
J1012+2439	1.81	27.6	2.41	2 bins/dec

Notes. The first and second columns report the name of the sources and their redshift, the third column the maximum photon energy, the fourth column the optical depth UL evaluated at 95% CL as $\tau_{\rm UL} = \ln[F_{\rm unabs}(E)/F_{\rm obs}(E)] + 2\sigma$, and the fifth column the number of energy bins/dec (for E>10 GeV) used to evaluate $F_{\rm obs}(E)$.

4. DISCUSSION

Studies with the highest energy extragalactic photons seen by the *Fermi*-LAT primarily probe the UV and optical components of the EBL. The background fields responsible for γ-ray attenuation can evolve strongly with redshift. In many of the models analyzed in this paper, the EBL intensity can exceed the local value by a factor of 10 or more at redshifts near the peak of star formation rate density. The optical depth to γ-rays from extragalactic sources is therefore determined by integrating the EBL intensity along the line of sight to the source from the observer.

For an interaction angle of $\theta = \pi$, the electron–positron pair production threshold condition leads to the value of the

[71] *gtlike* tool in the standard *Fermi*-LAT *Science Tools* package provided by the *Fermi* Science Support Center (FSSC).
[72] http://fermi.gsfc.nasa.gov/ssc/data/access/lat/BackgroundModels.html
[73] Since the energy bin is small enough to assume a flat spectrum.
[74] It has been verified that the statistical errors follow a Gaussian distribution. The standard error propagation formula has then been applied.

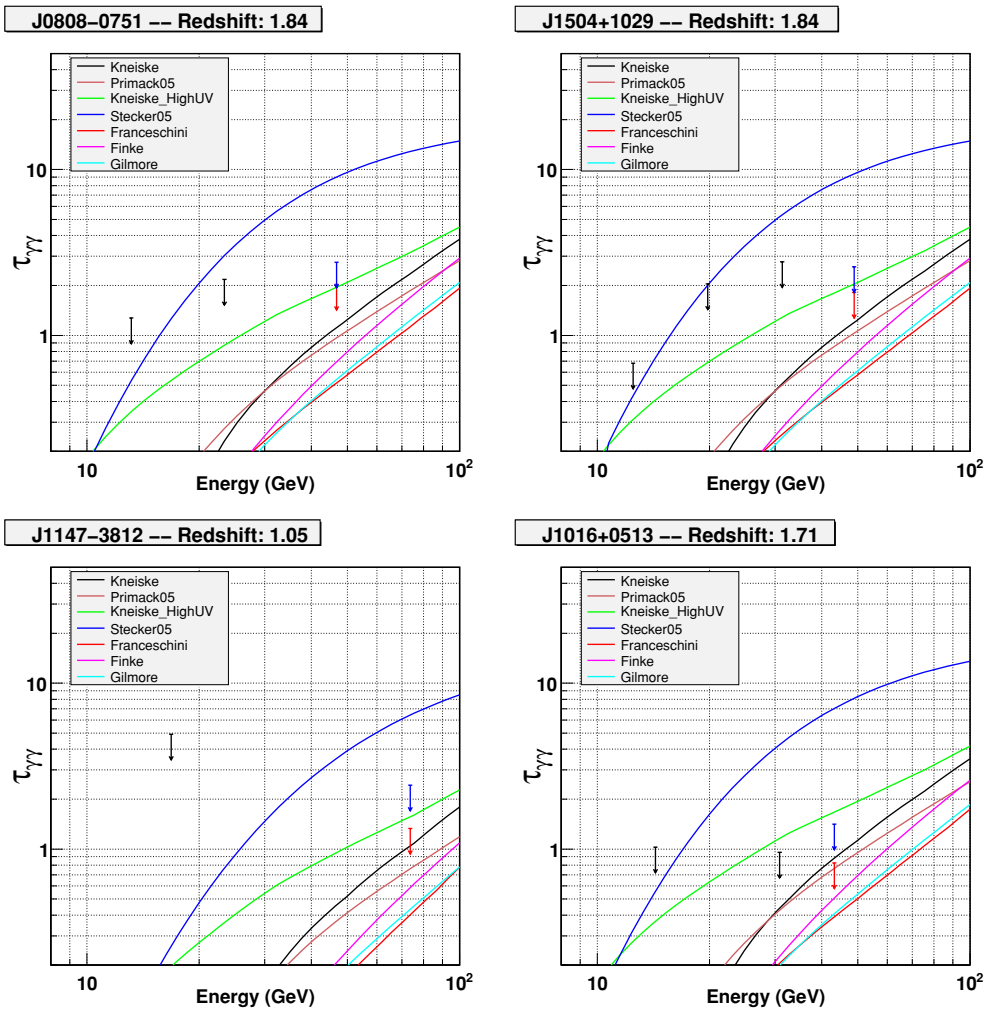

Figure 7. Derived upper limits for the optical depth of γ-rays emitted at $z = 1.84$ (J0808−0751, J1504+1029), $z = 1.05$ (J1147−3812), and $z = 1.71$ (J1016+0513). Black arrow (thin gray arrow in the print edition) upper limits at 95% CL in all energy bins used to determine the observed flux above 10 GeV. Red arrow (thick gray arrow in the print edition) upper limits at 95% CL for the highest energy photon. Blue arrow (thick black arrow in the print edition) upper limit at 99% CL for the highest energy photon. The upper limits are inconsistent with the EBL models that predict the strongest opacity.

(A color version of this figure is available in the online journal.)

longest wavelength photon with which a γ-ray emitted at $z_{\rm src}$ with observed energy $E_{\rm obs}$ can interact (source frame):

$$\lambda_{\rm max} = 47.5\,(1+z_{\rm src})\left[\frac{E_{\rm obs}}{\rm GeV}\right]\ \text{Å} \qquad (5)$$

The equation describes an UL on background photon wavelengths that can contribute to the γ-ray optical depth. Limits for $\lambda_{\rm max}$ include 7175 Å for blazar J1147−3812, and 4474 Å for GRB 090902B and 3286 Å for GRB 080916C, based on the highest energy γ-rays seen from these sources. In reality, interactions with shorter wavelength photons are more likely and will contribute more to the optical depth due to the redshifting of the γ-ray during propagation to Earth, the cross section, which peaks at approximately twice the threshold energy, and the geometry (interactions at angles of $\sim$90° are more likely than head-on interactions as used in Equation (5)).

The results of our analysis of the highest energy γ-rays from blazars and GRBs detected by the *Fermi*-LAT disfavor a UV background intensity at the level predicted both by the baseline and fast-evolution models of Stecker et al. (2006), although the LAT observations discussed here do not constrain the predictions of this work at longer wavelengths. The two models of this work are based upon a backward evolution model of galaxy formation. In this scenario, the IR SED of a galaxy is predicted from its luminosity at 60 μm. The locally determined 60 μm luminosity function is then assumed to undergo pure luminosity evolution following a power law in (1+z). Optical and UV luminosities, relevant to *Fermi*'s extragalactic observations, are then determined by analytic approximation to the SEDs in Salamon & Stecker (1998) and are normalized to the short wavelength portions of the IR SEDs. These models do not include absorption of UV light by dust in star-forming regions and the interstellar medium of galaxies, which may partially account for the high background in this model. While this model does account for redshift evolution in the UV-optical SEDs of galaxies, it does not allow for any evolution in the IR emission to which these SEDs are normalized. As mentioned by Stecker et al. (2006), this is another factor which could result in overpredicted UV emission.

Emissivity at UV wavelengths is closely tied to the global star formation rate density. Because the models of Stecker et al. (2006) are not derived from an assumed function for the star formation rate, limits on the UV emissivity in this case cannot be used to directly constrain star formation. We do not find that our results are conclusively in disagreement with the "best-fit"

model of Kneiske et al. (2004). In these models, the optical-UV EBL is based upon a Salpeter initial mass function and a star formation rate density that peaks at $z \sim 1.25$, with a value of $\sim 0.2\ M_{\odot}\ \mathrm{Mpc}^{-3}\ \mathrm{yr}^{-1}$, and falls slowly toward higher redshift. In the high-UV model, ultraviolet flux is boosted by a factor of 4 above the level of the best-fit model, greatly enhancing the opacity for γ-rays at energies below about 200 GeV. A star formation history of the magnitude required to produce the background in the high-UV model would be above essentially all estimates of the global star formation rate (see, for example, Hopkins & Beacom 2006). All other EBL models are of such low density in the UV range that they cannot be constrained by the data presented in this work. Although the results of our analysis cannot yet place any stringent ULs on the cosmological star formation history that are competitive with current observational estimates, future prospects for probing low density UV models of the EBL by means of improved methods and enlarged GeV photon data sets may be promising.

HE γ-rays that are absorbed by the EBL photons can initiate a pair cascade by subsequent Compton scattering of the CMB photons by the pairs. In case the intergalactic magnetic field (IGMF) is very weak, so that the pairs do not deflect out of our line of sight, this cascade radiation component can be detectable (Plaga 1995). Calculations of such cascade signatures have been carried out for AGNs (see, e.g., Dai et al. 2002; Murase et al. 2008; Essey & Kusenko 2010) and for GRBs (see, e.g., Dai & Lu 2002; Razzaque et al. 2004; Takahashi et al. 2008) and found to compensate for a large portion of the flux that is absorbed in the EBL. If blazars or GRBs are sources of ultrahigh energy cosmic rays (Waxman & Coppi 1996), then photohadronic interactions by protons during their propagation in the background light can also induce an HE cascade signature that would form appreciable HE emission, provided the IGMF is sufficiently small (Essey & Kusenko 2010). However, recent flux ULs calculated in the *Fermi*-LAT range from TeV blazars 1ES 0347−121 and 1ES 0229+200 constrain the IGMF to be $> 3 \times 10^{-16}$ G (Neronov & Vovk 2010). Such a strong field reduces the cascade flux significantly (because the emission becomes essentially isotropic due to the large deflection angles) and the contribution to the observed flux is likely to be small. Furthermore, since the constraining blazar sample consists of FSRQs only, which seem weak TeV emitters, any of their reprocessed emission can only be small also.

Exotic scenarios involving oscillation between γ-rays and axion-like particles, while propagating in the Galactic magnetic field, from distant sources may produce observable signatures in the TeV range (see, e.g., Mirizzi et al. 2007; Serpico 2009). However, the effect may not set in for typically assumed IGMF values or likely to be too small to make up for EBL flux attenuation in the $\lesssim$100 GeV range (see, e.g., Sanchez-Conde et al. 2009)

5. CONCLUSION

Using the HE 11 month photon data set collected by *Fermi* from distant blazars, and two GRBs we have (1) placed ULs on the opacity of the universe to γ-rays in the $\sim$10–100 GeV range coming from various redshifts up to $z \approx 4.3$; and (2) ruled out an EBL intensity in the redshift range $\sim$1 to 4.3 as great as that predicted by Stecker et al. (2006) in the ultraviolet range at more than 4σ post-trials in two independent sources (blazars). The overall rejection significance is found to be $> 10\sigma$ post-trials therefore making this result very robust. Our most constraining sources are blazars J1504+1029, J0808−0751 and J1016+0513 with $(z, \langle E_{\mathrm{max}} \rangle)$ combinations of (1.84, 48.9 GeV), (1.84, 46.8 GeV), and (1.71, 43.3 GeV), respectively. Although a likelihood ratio analysis of the latter source indicates that the sensitivity of our analysis method is approaching the EBL flux level of the "high UV model" of Kneiske et al. (2004), multi-trial effects markedly reduced the rejection significance. The two most constraining GRBs are GRB 090902B and GRB 080916C, both of which rule out the "baseline" EBL model of Stecker et al. (2006) in the UV energy range at more than 3σ level. The "fast-evolution" model of Stecker et al. (2006) predicts higher opacities in the LAT energy range at all redshifts and therefore is also ruled out. Together with the results from VHE observations (e.g., Aharonian et al. 2007; Mazin & Raue 2007), the models by Stecker et al. (2006) seem now disfavored in the UV and mid-IR energy range. We have also calculated model-independent optical depth ULs $\tau_{\gamma\gamma,\mathrm{UL}}(z, \langle E_{\mathrm{max}} \rangle)$ at 95% CL in the redshift $z \simeq$ 1–2.1 and $E_{\mathrm{max}} \approx$ 28–74GeV ranges.

As the HE photon data set collected by *Fermi* grows in the future and more blazars and GRBs are detected at constraining energies, the (E, z) phase space that constrains $\tau_{\gamma\gamma}$ will become more populated. This will provide us with unique opportunities to constrain the opacity of the universe to γ-rays over a large energy and redshift range, and eventually help us further understand the evolution of the intensity of the EBL over cosmic time.

The *Fermi*-LAT Collaboration acknowledges generous ongoing support from a number of agencies and institutes that have supported both the development and the operation of the LAT as well as scientific data analysis. These include the National Aeronautics and Space Administration and the Department of Energy in the United States, the Commissariat à l'Energie Atomique and the Centre National de la Recherche Scientifique/Institut National de Physique Nucléaire et de Physique des Particules in France, the Agenzia Spaziale Italiana and the Istituto Nazionale di Fisica Nucleare in Italy, the Ministry of Education, Culture, Sports, Science and Technology (MEXT), High Energy Accelerator Research Organization (KEK) and Japan Aerospace Exploration Agency (JAXA) in Japan, and the K. A. Wallenberg Foundation, the Swedish Research Council and the Swedish National Space Board in Sweden. Additional support for science analysis during the operations phase is gratefully acknowledged from the Istituto Nazionale di Astrofisica in Italy and the Centre National d'Études Spatiales in France. The *Fermi* GBM collaboration acknowledges support for GBM development, operations and data analysis from NASA in the US and BMWi/DLR in Germany. L.R.C. acknowledges support by the Kavli Institute for Cosmological Physics at the University of Chicago through grants NSF PHY-0114422 and NSF PHY-0551142 and an endowment from the Kavli Foundation and its founder Fred Kavli. A.R. acknowledges support by Marie Curie IRG grant 248037 within the FP7 Program. Furthermore, helpful comments from the referee are acknowledged.

REFERENCES

Abdo, A. A., et al. 2009a, Science, 323, 1688
Abdo, A. A., et al. 2009b, ApJ, 700, 597
Abdo, A. A., et al. 2009c, ApJ, 706, L138
Abdo, A. A., et al. 2010a, ApJ, 708, 1310
Abdo, A. A., et al. 2010b, ApJ, 710, 810
Abdo, A. A., et al. 2010c, ApJ, 710, 1271
Abdo, A. A., et al. 2010d, ApJ, 716, 30
Abdo, A. A., et al. 2010e, ApJ, 715, 429
Abdo, A. A., et al. 2010f, Phys. Rev. Lett., 104, 101101

Abdo, A. A., et al. 2010g, ApJ, 722, 520
Abdo, A. A., et al. 2010h, ApJS, 188, 405
Abdo, A. A., et al. 2010i, ApJ, 707, 1310
Abdo, A. A., et al. 2010j, ApJ, submitted
Acciari, V. A., et al. 2010, ApJ, 708, L100
Ackermann, M., et al. 2010, ApJ, 716, 1178
Aharonian, F. A., et al. 1999, A&A, 349, 11
Aharonian, F. A., et al. 2002, A&A, 384, 23
Aharonian, F. A., et al. 2006, Nature, 440, 1018
Aharonian, F. A., et al. 2007, A&A, 475, 9
Aharonian, F. A., Khangulyan, D., & Costamante, L. 2008, MNRAS, 387, 1206
Albert, J., et al. 2008, Science, 320, 1752
Atwood, W. B., et al. 2009, ApJ, 697, 1071
Band, D., et al. 1993, ApJ, 413, 281
Böttcher, M., Dermer, C. D., & Finke, J. D. 2008, ApJ, 679, L9
Chen, A., Reyes, L. C., & Ritz, S. 2004, ApJ, 608, 686
Costamante, L., Aharonian, F., Horns, D., & Ghisellini, G. 2004, New Astron. Rev., 48, 469
Dai, Z. G., & Lu, T. 2002, ApJ, 580, 1013
Dai, Z. G., Zhang, B., Gou, L. J., Mészáros, P., & Waxman, E. 2002, ApJ, 580, L7
Driver, S. P., Popescu, C. C., Tuffs, R. J., Graham, A. W., Liske, J., & Baldry, I. 2008, ApJ, 678, L101
Essey, W., & Kusenko, A. 2010, Astropart. Phys., 33, 81
Fazio, G. G., & Stecker, F. W. 1970, Nature, 226, 135
Finke, J. D., & Razzaque, S. 2009, ApJ, 698, 1761
Finke, J. D., Razzaque, S., & Dermer, C. D. 2010, ApJ, 712, 238
Fisher, R. A. 1925, Statistical Methods for Research Workers (Edinburgh: Oliver and Boyd)
Franceschini, A., Rodighiero, G., & Vaccari, M. 2008, A&A, 487, 837 (F08)
Georganopoulos, M., Sambruna, R. M., Kazanas, D., Cillis, A. N., Cheung, C. C., Perlman, E. S., Blundell, K. M., & Davis, D. S. 2008, ApJ, 686, L5
Greiner, J., et al. 2009, A&A, 498, 89
Gilmore, R. C., Madau, P., Primack, J. R., Somerville, R. S., & Haardt, F. 2009, MNRAS, 399, 1694
Gould, R. J., & Shréder, G. 1966, Phys. Rev. Lett., 16, 252
Hartmann, D. H. 2007, in AIP Conf. Proc. 921, The first GLAST Symp. ed. S. Ritz, P. Michelson, & C. A. Meegan (Melville, NY: AIP), 24
Hauser, M. G., & Dwek, E. 2001, ARA&A, 39, 249
Healey, S. E., Romani, R. W., Taylor, G. B., Sadler, E. M., Ricci, R., Murphy, T., Ulvestad, J. S., & Winn, J. N. 2007, ApJS, 171, 61
Healey, S. E., et al. 2008, ApJS, 175, 97
Hinton, J. A., & Hofmann, W. 2009, ARA&A, 47, 523
Hopkins, A. M., & Beacom, J. F. 2006, ApJ, 651, 142
Katarzyński, K., Ghisellini, G., Tavecchio, F., Gracia, J., & Maraschi, L. 2006, MNRAS, 368, L52
Kneiske, T. M., Bretz, T., Mannheim, K., & Hartmann, D. H. 2004, A&A, 413, 807
Kneiske, T. M., Mannheim, K., & Hartmann, D. H. 2002, A&A, 386, 1
Krennrich, F., Dwek, E., & Imran, A. 2008, ApJ, 689, L93
Madau, P., & Pozzetti, L. 2000, MNRAS, 312, L9
Marcha, M. J. M., Brown, I. W. A., Impey, C. D., & Smith, P. S. 1996, MNRAS, 281, 425
Massaro, E., Giommi, P., Leto, C., Marchegiani, P., Maselli, A., Perri, M., Piranomonte, S., & Sclavi, S. 2009, A&A, 495, 691
Massaro, E., Tramacere, A., Perri, M., Giommi, P., & Tosti, G. 2006, A&A, 448, 861
Mattox, J. R., Hartman, R. C., & Reimer, O. 2001, ApJS, 135, 155
Mattox, J. R., et al. 1996, ApJ, 461, 396
Mazin, D., & Raue, M. 2007, A&A, 471, 439
Mirizzi, A., Raffelt, G. G., & Serpico, P. D. 2007, Phys. Rev. D, 76, 023001
Murase, K., Takahashi, K., Inoue, S., Ichiki, K., & Nagataki, S. 2008, ApJ, 686, L67
Neronov, A., & Vovk, I. 2010, Science, 328, 73
Nishikov, A. I. 1961, Zh. Exp. Theo. Fiz., 41, 549
Plaga, R. 1995, Nature, 374, 430
Prandini, E., Bonnoli, G., Maraschi, L., Mariotti, M., & Tavecchio, F. 2010, MNRAS, 405, L65
Primack, J. R., Bullock, J. S., & Somerville, R. S. 2005, in AIP Conf. Proc. 745, High Energy Gamma-Ray Astronomy, ed. F. A. Aharonian, H. J. Völk, & D. Horns (Melville, NY: AIP), 23
Protassov, R., van Dyk, D. A., Connors, A., Kashyap, V. L., & Siemiginowska, A. 2002, ApJ, 571, 545
Razzaque, S., Dermer, C. D., & Finke, J. D. 2009, ApJ, 697, 483
Razzaque, S., Mészáros, P., & Zhang, B. 2004, ApJ, 613, 1072
Reimer, A. 2007, ApJ, 665, 1023
Salamon, M. H., & Stecker, F. W. 1998, ApJ, 493, 547
Sanchez-Conde, M. A., Paneque, D., Bloom, E. D., Prada, F., & Dominguez, A. 2009, Phys. Rev. D, 79, 123511
Schroedter, M. 2005, ApJ, 628, 617
Serpico, P. D. 2009, Adv. Space Sci., 43, 335
Stanev, T., & Franceschini, A. 1998, ApJ, 494, L159
Stecker, F. W., Baring, M. G., & Summerlin, E. J. 2007, ApJ, 667, L29
Stecker, F. W., & de Jager, O. C. 1993, ApJ, 415, L71
Stecker, F. W., Malkan, M. A., & Scully, S. T. 2006, ApJ, 648, 774 (St06; erratum, 658, 1392 [2007])
Stocke, J. T., et al. 1991, ApJ, 374, 72
Takahashi, K., Murase, K., Ichiki, K., Inoue, S., & Nagataki, S. 2008, ApJ, 687, L5
Tavani, M., et al. 2008, Nucl. Instrum. Methods Phys. Res. A, 588, 52
Tanvir, N. R., et al. 2009, Nature, 461, 1254
Thompson, D. J., et al. 1993, ApJS, 86, 629
Wagner, S. J., et al. (HESS Collaboration) 2010, BAAS, 41, 660
Waxman, E., & Coppi, P. 1996, ApJ, 464, L75
Wilks, S. S. 1938, Ann. Math. Stat., 9, 60